Hindawi
Advances in Materials Science and Engineering
Volume 2019, Article ID 5978149, 9 pages
https://doi.org/10.1155/2019/5978149

Research Article

Nanosized Zincated Hydroxyapatite as a Promising Heterogeneous Photo-Fenton-Like Catalyst for Methylene Blue Degradation

Van Dat Doan,[1] Van Thuan Le,[2] Thi Thanh Nhi Le,[2] and Hoai Thuong Nguyen[3,4]

[1]*Faculty of Chemical Engineering, Industrial University of Ho Chi Minh City, Ho Chi Minh City, Vietnam*
[2]*Center for Advanced Chemistry, Institute of Research & Development, Duy Tan University, Danang, Vietnam*
[3]*Division of Computational Physics, Institute for Computational Science, Ton Duc Thang University, Ho Chi Minh City, Vietnam*
[4]*Faculty of Electrical & Electronics Engineering, Ton Duc Thang University, Ho Chi Minh City, Vietnam*

Correspondence should be addressed to Hoai Thuong Nguyen; nguyenhoaithuong@tdtu.edu.vn

Received 21 January 2019; Accepted 28 March 2019; Published 24 April 2019

Guest Editor: Dinh Quang Khieu

This study is devoted to synthesis of nanosized zincated hydroxyapatite (Zn-HA) and its utilization as a heterogeneous photo-Fenton-like catalyst for degradation of methylene blue (MB) in aqueous solution. The prepared catalyst was characterized by various techniques such as X-ray diffraction, scanning electron microscopy, transmission electron microscopy, energy-dispersive X-ray, and Fourier transform infrared spectroscopy. The catalytic activity of Zn-HA towards MB and the effects of various experimental factors such as pH, zinc substitution degrees, initial MB concentration, and H_2O_2 dosage were studied in detail. The results showed that the zinc substitution degree of 0.4 is optimal to get the highest degradation efficiency under conditions of pH = 10, H_2O_2 dosage of 0.05 M, and MB concentration of 30 mg/L for a contact time of 120 min. The degradation mechanism was proposed and discussed thoroughly. Besides, the ability of long-term use for the synthesized catalyst was also evaluated.

1. Introduction

The rapid industrialization with developing various kinds of chemical-based industries leads to several major environmental issues caused by a huge amount of toxic substances discharged into ecosystems. In this context, persistent organic pollutants as dyes must be taken into account due to their high toxicity and nonbiodegradability under normal conditions [1–4]. Recently, an examination conducted in Singapore in 2017 reported that essential everyday foods such as vegetables, canned meat, fruits, and cheese in local supermarkets contained at least one type of azo dyes which might cause several health problems as lethal, genotoxic, mutagenic, and carcinogenic effects [5]. Thus, removal of toxic dyes from contaminated sources is extremely important and attracts a great attention from the global scientific community.

Up to now, there have been several methods used for removal of organic pollutants such as flocculation, ion-exchange, reverse osmosis, adsorption, etc. [6–8]. A major drawback of these methods is related to the secondary polluted compounds that can be generated since the separated pollutants are not destroyed after detoxification [9, 10]. To overcome this barrier, heterogeneous Fenton-photocatalysis has been utilized to remove organic pollutants by degrading them into eco-friendly biodegradable substances [11, 12]. In this photocatalysis, properties of photocatalysts play a leading role in ensuring success of a treatment process. In this regard, many kinds of Fenton-photocatalysts have been developed. Among them, heterogeneous photocatalysts containing transition metals such as Fe, Cu, Zn, Mn, Co, Mn, and Ti are widely used due to their high photocatalytic activity and low cost [11, 13]. However, these materials exhibit a good performance mostly in UV region, but not under a wide spectrum of visible light due to the limits of their band gaps [14–16]. Moreover, most of the methods used to modify band gaps for improving

photocatalytic activity of catalysts are quite expensive and complicated [17–20].

Recently, several studies have been made on using hydroxyapatite ($Ca_{10}(PO_4)_6(OH)_2$-HA), a main mineral constituent of mammalian hard tissues, as a supporting material for improving photocatalytic activity of catalysts because of its biocompatibility and excellent adsorption capacity and photocatalytic activity for removal of both organic compounds and toxic heavy metals [21–24]. With regards to photocatalytic activity, Valizadeh et al. have successfully synthesized magnetite-hydroxyapatite for photocatalytic degradation of acid blue 25 [24]. Besides, another research group [25] used waste mussel shells to develop HA as a greener and renewable photocatalyst for the degradation of methylene blue (MB) [25]. Although the photocatalytic capacity of HA is not higher than those of metal-oxide photocatalysts, cost benefits, eco-friendliness, simple preparation, and reusability are huge advantages of this material. Especially, the structure of HA can be modified because its cations Ca^{2+} and functional groups of PO_4^{3-} and OH^- are easily replaced by other ions, and therefore, its photocatalytic potential can be intervened. For example, Fe_3O_4-hydroxyapatite modified by Mn, Fe, Co, Ni, Cu, and Zn as reported in [26] exhibited very high photocatalytic capability towards dyes in water under UV irradiation. However, there have been several drawbacks that are needed to overcome. Firstly, the Fe_3O_4 and hydroxyapatite components were physically linked to each other, leading to the low stability of material structure during a long-term treatment process. Secondly, the used metals were distributed mainly inside Fe_3O_4-hydroxyapatite structure, but not on its surface due to the substitution of Ca^{2+} by metals ions took place mainly at lattice points [26, 27]. As a result, Fe_3O_4-hydroxyapatite could not be able to exhibit its full photocatalytic potential.

Based on the above arguments, this study is devoted to using chemical precipitation method to develop a single-phase Zn-HA as a heterogenous photo-Fenton-like catalyst for MB degradation. For this material, Zn is integrated into HA via anion substitution of PO_4^{3-} by $Zn(OH)_4^{2-}$. Crystalline structure, morphology, features of functional groups, and element analysis of Zn-HA were carefully characterized using XRD, SEM, TEM, FTIR, and EDX techniques. Besides, the optimal conditions for degradation of MB were also determined. Finally, the reusability was also evaluated for the long-term of the catalyst.

2. Materials and Methods

2.1. Reagents and Materials. Calcium hydroxide ($Ca(OH)_2$, ≥96%), phosphoric acid (H_3PO_4, 85%), sodium hydroxide (NaOH, 99%), zinc oxide (ZnO, 99%), MB ($C_{16}H_{18}ClN_3S$, ≥82%), hydrogen peroxide (H_2O_2, 30%), and ammonium hydroxide (NH_4OH, 30%) were reagent-grade, supplied by Merck chemical company (Germany), and used without further purification. Distilled water was used to prepare all necessary solutions for the synthesis of Zn-HA.

2.2. Preparation of Zn-HA Catalyst. The Zn-HA samples were synthesized by the chemical precipitation method from solutions of $Na_2Zn(OH)_4$, $Ca(OH)_2$, and H_3PO_4. The solution of $Na_2Zn(OH)_4$ was prepared by adding gradually 0.2 M NaOH solution into a suspension of 0.05 M ZnO until a clear solution was obtained. The solutions of 0.02 M $Ca(OH)_2$ and H_3PO_4 10% were prepared from pure solid of $Ca(OH)_2$ and concentrated solution of H_3PO_4 85%, respectively. For the synthesis of Zn-HA, the solution of H_3PO_4 10% was slowly added drop by drop into a reactor containing $Na_2Zn(OH)_4$ and $Ca(OH)_2$ with vigorous stirring for 1 h. The solutions were taken out at different Ca : P : Zn ratios of 9 : 6 : 0; 9 : 5.9 : 0.1; 9 : 5.75 : 0.25; 9 : 5.6 : 0.4; 9 : 5.4 : 0.55; and 9 : 5.3 : 0.65 named as HA, Zn-HA-0.1, Zn-HA-0.25, Zn-HA-0.4, Zn-HA-0.55, and Zn-HA-0.65, respectively. The pH of obtained solutions was kept at pH ≥ 10 using NH_4OH. After the reactions finished, the mixtures were left for aging at room temperature for 24 h and then filtered, washed, dried, crushed, and pulverized through a 100-mesh sieve.

2.3. Characterization of Catalysts. X-ray powder diffraction (XRD) on a Shimadzu 6100 diffractometer (Japan) with Cu target ($\lambda = 1.5406$ Å), accelerating voltage of 40 kV, and current stream of 30 mA in a scanning range from 5 to 90° at a speed of 0.05°/s with a step size of 0.02° was used to explore structural properties of materials. The features of functional groups were analyzed by Fourier transform infrared spectroscopy (FTIR) technique on a Tensor 27 spectrophotometer (Germany) in a scanning range from 500–4000 cm^{-1} using KBr pellet method. The morphology of materials was tested by the methods of scanning electron microscopy (SEM) and transmission electron microscopy (TEM) on Jeol JSM-6480 LV and Jeol 1400 (Japan) microscopes, respectively. Finally, energy-dispersive X-ray (EDX) and element mapping techniques were utilized on a Horiba 7593 dispersive X-ray microanalyzer (Japan) to analyze the chemical elemental characteristics of the obtained materials.

2.4. Experiments for MB Degradation. The photo-Fenton catalytic potential of the as-prepared Zn-HA composite was evaluated through the degradation of MB as a model azo dye. A certain amount of catalyst was dispersed into 100 mL of MB solution (20, 30, 50, 80, 100 mg/L) and stirred in the dark for 30 min to reach adsorption-desorption equilibrium between MB and catalyst. Then, a calculated amount of H_2O_2 was added into the suspension to initiate the reaction under light irradiation turned on at the same time from 250 W halogen lamp (HLX 64653; Osram, Germany, wavelength range of 300–800 nm) equipped with a 420 nm cut-off filter. Besides, a thermostatic water-bath was employed to keep the reaction temperature at a desired value. In addition, the initial pH of MB solutions was adjusted to a desired value using 0.1 M NaOH or 0.1 M HCl solutions. After each 10-minute contact time, 2 mL of the mixture was taken out, the catalyst was then eliminated by centrifugation, and the remaining MB concentration was analyzed using an Evolution 600 UV-visible spectrophotometer at $\lambda_{max} = 664$ nm. The influence of factors as initial pH, catalyst dosage, initial

hydrogen peroxide dosage, MB concentration, and zinc content on the MB degradation was carefully examined. The efficiency for degradation of MB using Zn-HA is calculated by the following formula:

$$R_e = \frac{C_0 - C_f}{C_0} \cdot 100, \quad (1)$$

where R_e (%) is the removal efficiency and C_0(mg/L) and C_f(mg/L) are the initial and final concentrations of MB solution before and after degradation, respectively.

Photocatalytic stability and reusability of the catalysts were evaluated by testing the photocatalytic degradation efficiency of MB in five consecutive cycles, each cycle lasted 60 min. After each cycle, the photocatalyst was centrifuged and then added again into fresh MB solution (100 mL, 50 mg/L, pH of 10, H_2O_2 dosage of 0.05 M) for the next round.

3. Results and Discussion

3.1. Characterization of the Catalyst. The results for study on crystalline structures of HA and Zn-HA with different Zn content are shown in Figure 1.

It is obviously seen that the XRD patterns of Zn-HA samples contain all characteristic peaks for HA at 2θ of 10.8, 25.7, 28.2, 29.1, 31.7, 32.8, 39.7, 46.9, 48, 49.5, and 53.1° (ICD PDF 00-024-0033). In other words, the zinc doping did not affect crystalline structure of HA. Similar results were also reported in previous studies [28–30]. However, as compared to the HA, the peaks obtained for Zn-HA are broadened. This might be due to the decrease in the crystallinity and particle size of the Zn-HA sample [30]. Besides, the XRD patterns also indicated that there were additional phases of $Ca(OH)_2$ and $CaCO_3$ detected in Zn-HA samples at a zinc substitution degree higher than 0.4 (Figure 1). This anomaly can be explained as follows. The increase in the amount of $Zn(OH)_4^{2-}$ (which was made by the dissolution of ZnO in NaOH as described above) in the reaction mixture of $Ca(OH)_2$ and H_3PO_4 led to the shortage of H_3PO_4 due to its neutralization by NaOH and therefore resulting in the superabundance of $Ca(OH)_2$. At the same time, a part of extra $Ca(OH)_2$ could react with CO_2 in atmosphere to form $CaCO_3$.

The morphology of HA and Zn-HA at Zn-substitution degree of 0.4 is presented in Figure 2. It can be seen that the crystals of HA were grown in needle shape with 150–200 nm length and 30–50 nm width (Figure 2(a)) while Zn-HA crystals have a spherical shape with a diameter of about 20 nm (Figure 2(b)). The difference of size and shape between HA and Zn-HA might be associated with the increased number of crystallization centers when $Zn(OH)_4^{2-}$ was added into the reaction mixture of $Ca(OH)_2$ and H_3PO_4. Consequently, more crystals might be formed, leading to the decrease in their size. This is also in good agreement with the above XRD patterns. It should be noticed that the smaller the size of crystals, the larger the specific surface area obtained. This feature is an advantage of Zn-HA over HA towards photocatalytic ability. On a larger-scale view as shown in SEM images (Figures 2(c) and 2(d)), both HA and Zn-HA show a similar morphology.

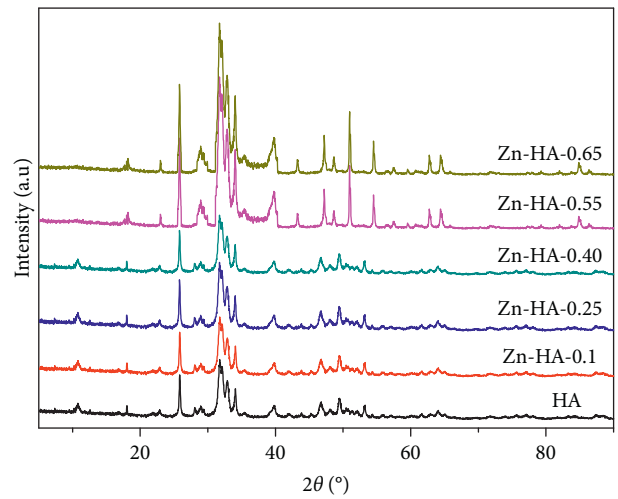

Figure 1: XRD patterns of HA and Zn-HA samples with different Zn content.

The doping of Zn into HA was also confirmed by EDX spectra and element mapping as shown in Figure 3. According to the EDX spectrum for Zn-HA (Figure 3(b)), along with the main elements characteristic for HA such as Ca, P, and O (Figure 3(a)), Zn was detected. Besides, the contents of Ca, P, and O elements in HA and Zn-HA are different. Comparing with HA, the content of P and O in Zn-HA was found to decrease from 13.77 to 2.41 w% and 59.97 to 50.01 w%, respectively. Meanwhile, the Ca content increased from 23.81 to 44% equal to the Ca content in stoichiometric HA. It obviously indicated that PO_4^{3-} groups in HA were partially replaced by $Zn(OH)_4^{2-}$. Moreover, the element mapping shows also the appearance of 4 elements of Ca, Zn, O and P on Zn-HA (Figures 3(c)–3(f)). In addition, the even distribution of Zn ions on Zn-HA surface (Figure 3(d)) is expected to improve photocatalytic activity of the synthesized catalyst as compared to those of HA.

The results for study on features of functional groups for HA and Zn-HA with different Zn content are shown in Figure 4. It is obviously seen that FTIR spectra obtained for HA and Zn-HA have a similar shape and most of characteristic peaks as 1030, 1085, 956, and 874 cm^{-1} referred to OH^- were detected at the same positions. Besides, the presence of CO_3^{2-} as mentioned above was also detected at 1650 and 1423 cm^{-1}. However, a difference of intensity between some peaks in HA and Zn-HA was observed. Specifically, for Zn-HA samples, the intensity of a peak at 3640 cm^{-1} (OH^- groups) was found to be increased and at 1030 cm^{-1} (PO_4^{3-} groups) decreased in comparison with those for HA, confirming the successful integration of $Zn(OH)_4^{2-}$ into HA structure.

3.2. Photo-Fenton Catalytic Activity of the Catalysts. In order to evaluate the photocatalytic advantage of Zn-HA over HA, a comparative study was conducted under the same experimental conditions of light irradiation, pH = 10, and catalyst loading of 0.1 g added into 100 mL of 50 mg·L^{-1} MB solution at room temperature. The Fenton-photocatalytic activity of catalysts was tested by adding 0.05 M H_2O_2 into

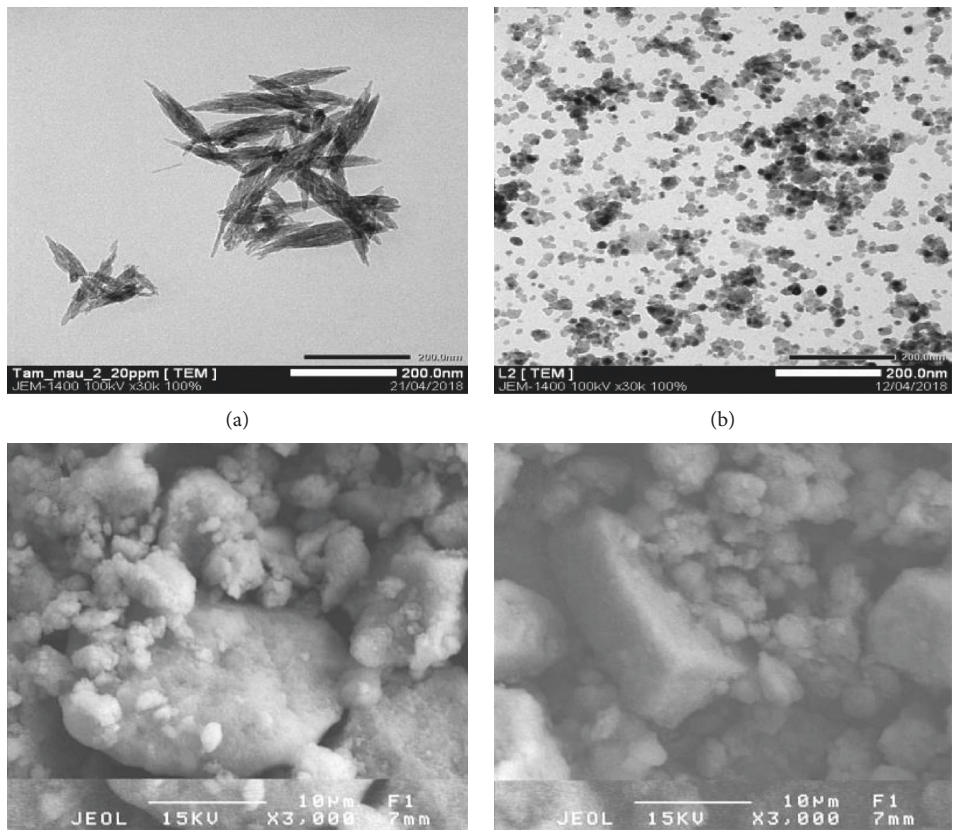

(a) (b)

(c) (d)

Figure 2: TEM and SEM images for HA (a, c) and Zn-HA (b, d).

the MB solution. As seen in Figure 5, when H_2O_2 was absent, the removal efficiencies obtained for both Zn-HA and HA were quite low as compared to those with the participation of H_2O_2. Besides, the maximum degradation efficiency of Zn-HA was much higher than that of HA for both cases with presence of H_2O_2 and absence of H_2O_2 (Figure 5). Obviously, the removal process in the absence of H_2O_2 was controlled mainly by adsorption mechanism, and therefore, the smaller size of Zn-HA helps it to take advantage over HA. In the presence of H_2O_2, along with adsorption mechanism, the Fenton-photocatalytic reactions could be activated and improved the degradation process. In this regard, the higher degradation efficiency of Zn-HA than that of HA indicated its stronger Fenton-photocatalytic potential. In other words, the presence of Zn could significantly improve the Fenton-photocatalytic ability of HA.

The photodegradation mechanism can be formulated as follows. Under visible light irradiation, electron/hole pairs were photogenerated in the catalyst (equation (2)). Then, photogenerated electrons could be trapped by H_2O_2, leading to the formation of $^{\cdot}OH$ (equation (3)) [31]. At the same time, Zn^{2+} ions after occupying electrons (equations (4)) were transformed into Zn which reacted with H_2O_2 to form ZnO, a strong photocatalyst (equation (5)) [32]. During light irradiation, ZnO was capable of creating more electrons and holes (equation (6)), and therefore, the decomposition process of H_2O_2 to release $^{\cdot}OH$ will be accelerated due to the support of electrons (equation (8)). In addition, the generated electrons could also stimulate the formation of superoxide radicals through reactions with dissolved oxygen in the solution (equation (7)). Meanwhile, the holes could also contribute to the formation of $^{\cdot}OH$ when reacting with H_2O and OH^- (equations (8) and (9)). Finally, $^{\cdot}OH$ and $^{\cdot}O_2^-$ will degrade MB molecules according to equations (10) and (11) [33].

$$\mathrm{Zn-HA} + h\nu \longrightarrow \mathrm{Zn-HA} + e^- + h^+ \quad (2)$$

$$\mathrm{H_2O_2} + e^- \longrightarrow {}^{\cdot}\mathrm{OH} + \mathrm{OH^-} \quad (3)$$

$$\mathrm{Zn^{2+}} + 2e^- \longrightarrow \mathrm{Zn} \quad (4)$$

$$\mathrm{Zn} + \mathrm{H_2O_2} \longrightarrow \mathrm{ZnO} + \mathrm{H_2O} \quad (5)$$

$$\mathrm{ZnO} + h\nu \longrightarrow e^- + h^+ \quad (6)$$

$$e^- + \mathrm{O_2} \longrightarrow {}^{\cdot}\mathrm{O_2^-} \quad (7)$$

$$h^+ + \mathrm{H_2O} \longrightarrow \mathrm{H^+} + {}^{\cdot}\mathrm{OH} \quad (8)$$

$$h^+ + \mathrm{OH^-} \longrightarrow {}^{\cdot}\mathrm{OH} \quad (9)$$

$$^{\cdot}\mathrm{OH} + \mathrm{MB} \longrightarrow \text{degradation products} \quad (10)$$

$$^{\cdot}\mathrm{O_2^-} + \mathrm{MB} \longrightarrow \text{degradation products} \quad (11)$$

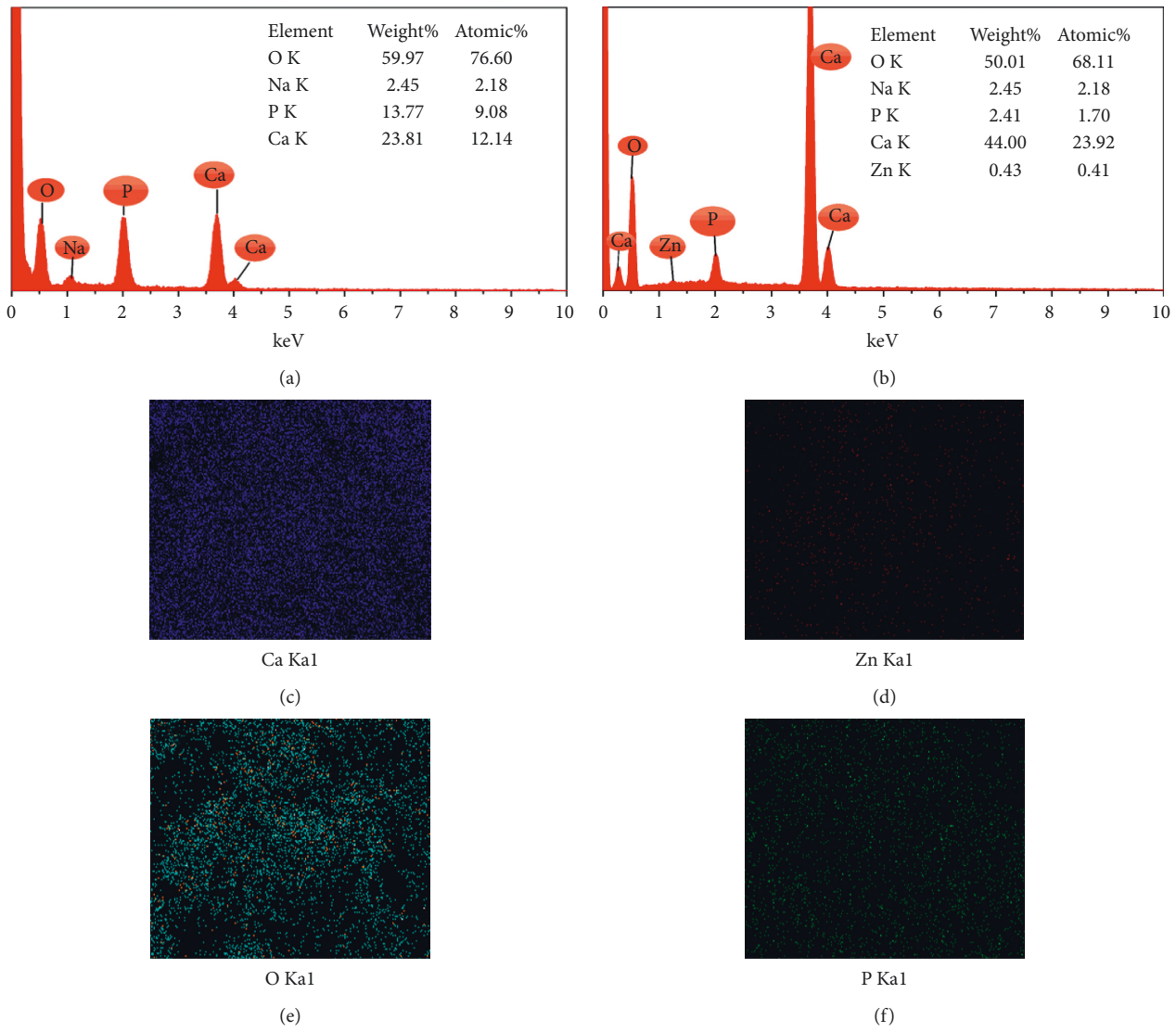

Figure 3: EDX patterns of HA (a) and Zn-HA (b), and element distribution on Zn-HA surface for calcium (c), zinc (d), oxygen (e), and phosphorus (f).

Although the above results indicated the advantage of Zn in enhancing Fenton-photocatalytic activity of Zn-HA over HA, the optimum content of Zn is needed to be determined. For this purpose, a comparative study on catalytic activity of Zn-HA samples with different zinc substitution degrees under the same degradation conditions as mentioned. The results showed that the zinc substitution degree of 0.4 gave the highest degradation efficiency of 95% after a contact time of 30 min as shown in Figure 6. In this regard, the obtained value of 0.4 is reasonable and was chosen for further experiments.

3.3. Influence of Experimental Conditions on MB Degradation

3.3.1. Effect of pH. Effect of pH on degradation efficiency of Zn-HA was studied in pH range from 4 to 10 using 0.1 g of Zn-HA added into 100 mL solution of 50 mg/L MB and 0.05 M H_2O_2. The obtained results are presented in Figure 7(a). It is obviously seen that the degradation efficiency significantly increased with increasing solution pH. This can be explained by the increased amount of OH^- groups, leading to rise in the amount of $^{\cdot}OH$ radicals generated through Fenton-oxidation mechanism, and therefore the degradation process was improved [13]. The fact that increasing pH greater than 10 does not make sense for practical applications since there is no economic benefit and the secondary pollutants could be generated at high pH. In this regard, pH = 10 was chosen as an optimal pH for all catalytic experiments in this work.

3.3.2. Effect of Initial MB Concentrations. Different initial MB concentrations of 20, 30, 50, 80, and 100 mg/L were used to evaluate their effect on degradation efficiency of Zn-HA catalyst under pH of 10, catalyst dosage of 0.1 g, and

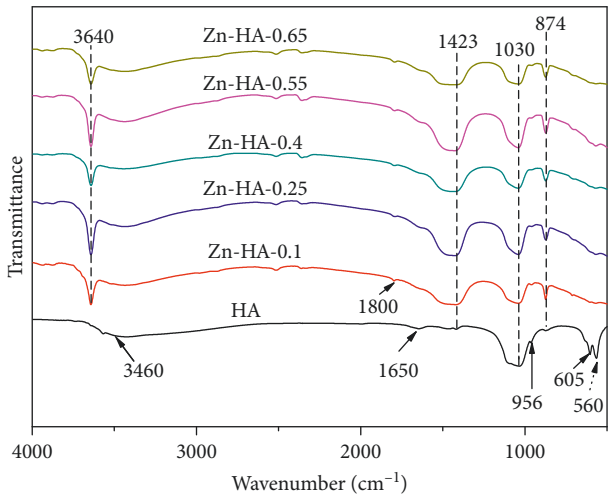

Figure 4: FTIR spectra for HA and Zn-HA samples with different Zn content.

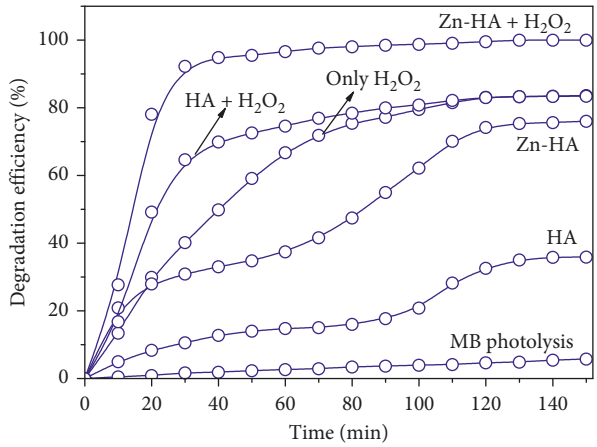

Figure 5: Comparative study on catalytic activity of the HA and Zn-HA for degradation of MB.

H_2O_2 dosage of 0.05 M at room temperature. Based on the obtained results, the optimal initial MB concentration was determined as 30 mg/L (Figure 7(b)). At concentrations higher than 30 mg/L, the reduction of degradation efficiency was observed. The anomaly could be related to the formation of a layer of MB molecules accumulated on Zn-HA surface at high MB concentrations, inhibiting light from entering Zn sites and therefore holding back the decolorization process [34].

3.3.3. Effect of H_2O_2 Concentration. The study was carried out using different initial H_2O_2 concentrations of 0.01, 0.03, 0.05, and 0.10 M under the established above optimal conditions. According to the results shown in Figure 7(c), the initial H_2O_2 concentration of 0.05 M is optimal for degradation of MB using Zn-HA. The deviation of initial H_2O_2 concentration from 0.05 M did not improve degradation process. It is obviously seen that at H_2O_2 concentrations lower 0.05 M, the reduction of

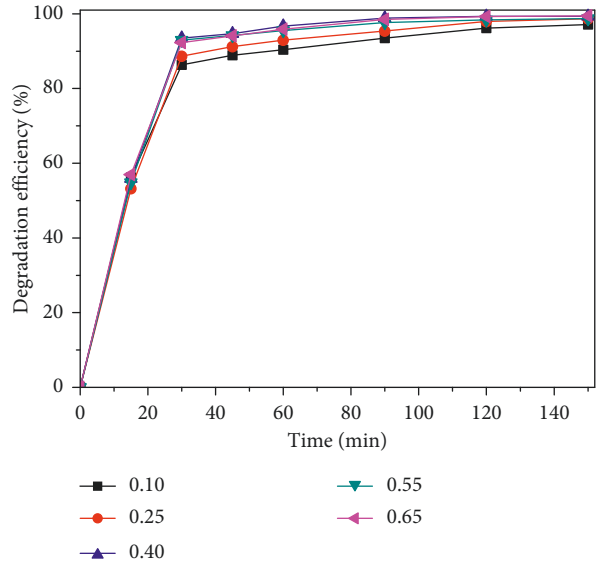

Figure 6: Comparative study on catalytic activity of Zn-HA samples with different zinc substitution degrees.

degradation efficiency could be associated with the decrease in the number of generated $^{\cdot}OH$ radicals. Meanwhile, at H_2O_2 concentrations greater than 0.05 M, the degradation efficiency did not increase (Figure 7(c)), probably, due to the generation of perhydroxyl radicals caused by the combination of extra H_2O_2 dosage with hydroxyl radicals [35].

3.4. Stability and Reusability of Catalyst. The stability and reusability of a catalyst are essential for its practical applications. For Zn-HA catalyst, the recycling tests were carried out under optimal conditions in five continuous cycles. The results shown in Figure 8(a) indicated that the catalytic potential of Zn-HA towards MB was well maintained with a slight reduction of degradation efficiency from 100% to 96.5% after five continuous cycles. Besides, the XRD pattern of Zn-HA after the fifth degradation cycle contained almost all characteristic peaks (Figure 8(b)), demonstrating high stability of composite structure during degradation process.

4. Conclusions

In this study, the nanosized Zn-HA was successfully synthesized and applied as a heterogeneous photo-Fenton-like catalyst for MB degradation under optimal conditions of pH = 10, H_2O_2 dosage of 0.05 M, and MB concentration of 30 mg/L for a contact time of 120 min. Besides, the zinc substitution degree of 0.4 is optimal to improve the photocatalytic activity of the catalyst. The recycling study demonstrated a good maintenance of degradation ability and high stability of catalyst structure in a long-term degradation process. Overall, the positive results suggested that the synthesized catalyst can be expected as a promising heterogeneous photocatalyst for degradation of MB in industrial wastewater.

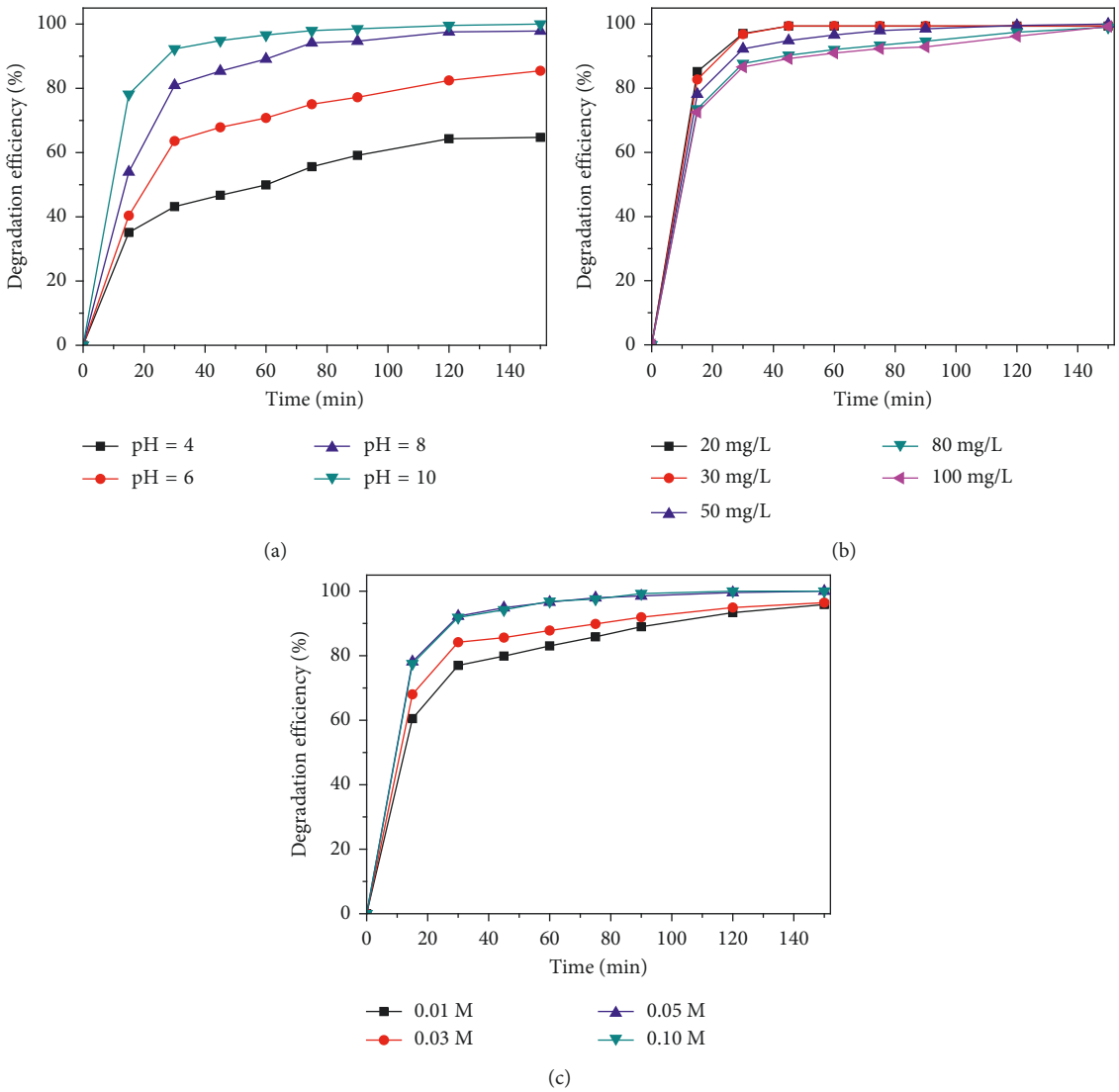

Figure 7: Effects of degradation conditions on degradation efficiency of Zn-HA sample. (a) pH. (b) Initial MB concentration. (c) Initial H_2O_2 concentration.

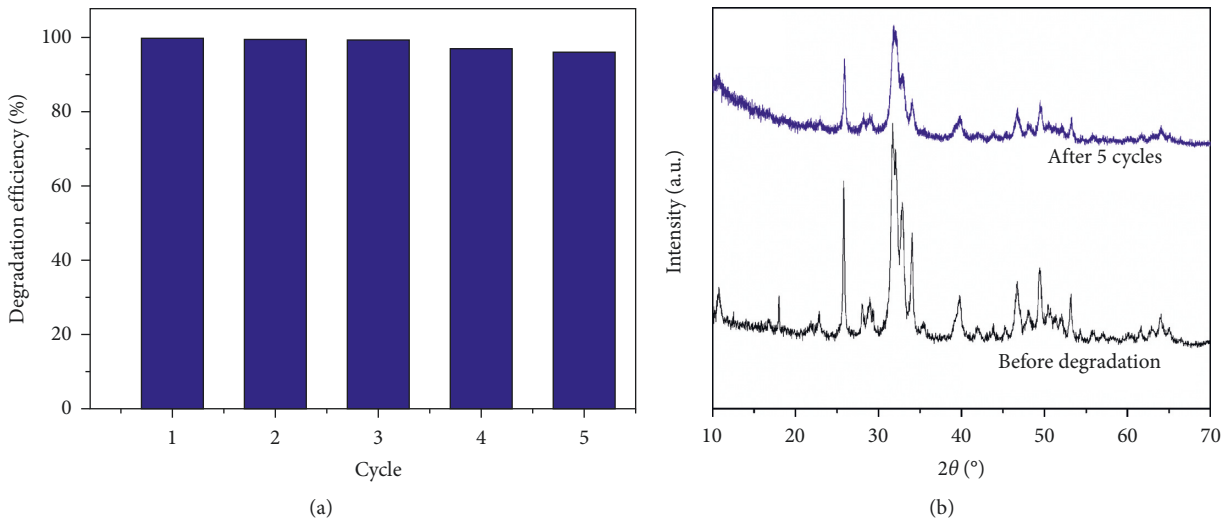

Figure 8: Degradation efficiency reduction (a) and the change of XRD pattern (b) of Zn-HA after for continuous cycles.

Data Availability

The all data used to support the findings of this study are included within the article.

Conflicts of Interest

The authors declare that they have no conflicts of interest.

Acknowledgments

The authors acknowledge the Industrial University of Ho Chi Minh City, Vietnam, for supporting this work (Funding No. 184.HHO5).

References

[1] V. Katheresan, J. Kansedo, and S. Y. Lau, "Efficiency of various recent wastewater dye removal methods: a review," *Journal of Environmental Chemical Engineering*, vol. 6, no. 4, pp. 4676–4697, 2018.

[2] H. Mittal, S. M. Alhassan, and S. S. Ray, "Efficient organic dye removal from wastewater by magnetic carbonaceous adsorbent prepared from corn starch," *Journal of Environmental Chemical Engineering*, vol. 6, no. 6, pp. 7119–7131, 2018.

[3] T. T. T. Tran, V. D. Doan, T. T. T. Ho, V. T. Le, and H. T. Nguyen, "Novel of TiO_2/Ag_3PO_4/bentonite composite photocatalyst: preparation, characterization, and application for degradation of methylene blue in aqueous solution," *Environmental Engineering Science*, vol. 36, no. 1, pp. 71–80, 2019.

[4] K.-T. Chung, "Azo dyes and human health: a review," *Journal of Environmental Science and Health, Part C*, vol. 34, no. 4, pp. 233–261, 2016.

[5] L. Leo, C. Loong, X. L. Ho, M. F. B. Raman, M. Y. T. Suan, and W. M. Loke, "Occurrence of azo food dyes and their effects on cellular inflammatory responses," *Nutrition*, vol. 46, pp. 36–40, 2018.

[6] L. Tang, J. Yu, Y. Pang et al., "Sustainable efficient adsorbent: alkali-acid modified magnetic biochar derived from sewage sludge for aqueous organic contaminant removal," *Chemical Engineering Journal*, vol. 336, pp. 160–169, 2018.

[7] M. Wawrzkiewicz and Z. Hubicki, "Anion exchange resins as effective sorbents for removal of acid, reactive, and direct dyes from textile wastewaters," in *Ion Exchange-Studies and Applications*, IntechOpen, London, UK, 2015.

[8] M. T. Yagub, T. K. Sen, S. Afroze, and H. M. Ang, "Dye and its removal from aqueous solution by adsorption: a review," *Advances in Colloid and Interface Science*, vol. 209, pp. 172–184, 2014.

[9] P. Zhao, S. Li, J. Zhao, C. M. Gaspar, and X. Weng, "Training by visual identification and writing leads to different visual word expertise N170 effects in preliterate Chinese children," *Developmental Cognitive Neuroscience*, vol. 15, pp. 106–116, 2015.

[10] S. De Gisi, G. Lofrano, M. Grassi, and M. Notarnicola, "Characteristics and adsorption capacities of low-cost sorbents for wastewater treatment: a review," *Sustainable Materials and Technologies*, vol. 9, pp. 10–40, 2016.

[11] R. Ameta, A. K. Chohadia, A. Jain, and P. B. Punjabi, "Fenton and photo-fenton processes," in *Advanced Oxidation Processes for Waste Water Treatment*, S. C. Ameta and R. Ameta, Eds., pp. 49–87, Academic Press, Cambridge, MA, USA, 2018, ISBN 9780128104996.

[12] A. Mirzaei, Z. Chen, F. Haghighat, and L. Yerushalmi, "Removal of pharmaceuticals from water by homo/heterogonous Fenton-type processes—a review," *Chemosphere*, vol. 174, pp. 665–688, 2017.

[13] S. Kalal, A. Pandey, R. Ameta, and P. B. Punjabi, "Heterogeneous photo-Fenton-like catalysts $Cu_2V_2O_7$ and $Cr_2V_4O_{13}$ for an efficient removal of azo dye in water," *Cogent Chemistry*, vol. 2, no. 1, article 1143344, 2016.

[14] B. Palas, G. Ersöz, and S. Atalay, "Photo Fenton-like oxidation of Tartrazine under visible and UV light irradiation in the presence of $LaCuO_3$ perovskite catalyst," *Process Safety and Environmental Protection*, vol. 111, pp. 270–282, 2017.

[15] Y. He, D. B. Jiang, D. Y. Jiang, J. Chen, and Y. X. Zhang, "Evaluation of MnO_2-templated iron oxide-coated diatomites for their catalytic performance in heterogeneous photo Fenton-like system," *Journal of Hazardous Materials*, vol. 344, pp. 230–240, 2018.

[16] M. S. Vasilyeva, V. S. Rudnev, A. A. Zvereva et al., "FeOx,SiO_2,TiO_2/Ti composites prepared using plasma electrolytic oxidation as photo-Fenton-like catalysts for phenol degradation," *Journal of Photochemistry and Photobiology A: Chemistry*, vol. 356, pp. 38–45, 2018.

[17] Y. Zhu, R. Zhu, L. Yan et al., "Visible-light Ag/AgBr/ferrihydrite catalyst with enhanced heterogeneous photo-Fenton reactivity via electron transfer from Ag/AgBr to ferrihydrite," *Applied Catalysis B: Environmental*, vol. 239, pp. 280–289, 2018.

[18] A. Zhang, L. Zhu, and Z. Nan, "Ni-doped Fe_3O_4 nanoparticles coupled with SnS_2 nanosheets as 0D/2D heterogeneous catalyst for photo-Fenton reaction," *Materials Chemistry and Physics*, vol. 224, pp. 156–168, 2019.

[19] L. Yu, J. Chen, Z. Liang, W. Xu, L. Chen, and D. Ye, "Degradation of phenol using Fe_3O_4-GO nanocomposite as a heterogeneous photo-Fenton catalyst," *Separation and Purification Technology*, vol. 171, pp. 80–87, 2016.

[20] C. Liang, Y. Liu, K. Li et al., "Heterogeneous photo-Fenton degradation of organic pollutants with amorphous Fe-Zn-oxide/hydrochar under visible light irradiation," *Separation and Purification Technology*, vol. 188, pp. 105–111, 2017.

[21] V. T. Le, V. D. Doan, D. D. Nguyen et al., "A novel cross-linked magnetic hydroxyapatite/chitosan composite: preparation, characterization, and application for Ni(II) ion removal from aqueous solution," *Water, Air, & Soil Pollution*, vol. 229, no. 3, p. 101, 2018.

[22] L. V. Thuan, D. V. Dat, P. C. Nguyen, and M. A. Trubitsyn, "Synthesis of calcium-deficient carbonated hydroxyapatite as promising sorbent for removal of lead ions," *Journal of Nano Research*, vol. 45, pp. 124–133, 2017.

[23] W. Liu, G. Qian, B. Zhang, L. Liu, and H. Liu, "Facile synthesis of spherical nano hydroxyapatite and its application in photocatalytic degradation of methyl orange dye under UV irradiation," *Materials Letters*, vol. 178, pp. 15–17, 2016.

[24] S. Valizadeh, M. H. Rasoulifard, and M. S. S. Dorraji, "Modified Fe_3O_4-hydroxyapatite nanocomposites as heterogeneous catalysts in three UV, Vis and Fenton like degradation systems," *Applied Surface Science*, vol. 319, pp. 358–366, 2014.

[25] J. H. Shariffuddin, M. I. Jones, and D. A. Patterson, "Greener photocatalysts: hydroxyapatite derived from waste mussel shells for the photocatalytic degradation of a model azo dye wastewater," *Chemical Engineering Research and Design*, vol. 91, no. 9, pp. 1693–1704, 2013.

[26] A. Fihri, C. Len, R. S. Varma, and A. Solhy, "Hydroxyapatite: a review of syntheses, structure and applications in

heterogeneous catalysis," *Coordination Chemistry Reviews*, vol. 347, pp. 48–76, 2017.

[27] M. Ferri, S. Campisi, M. Scavini, C. Evangelisti, P. Carniti, and A. Gervasini, "In-depth study of the mechanism of heavy metal trapping on the surface of hydroxyapatite," *Applied Surface Science*, vol. 475, pp. 397–409, 2019.

[28] E. S. Thian, T. Konishi, Y. Kawanobe et al., "Zinc-substituted hydroxyapatite: a biomaterial with enhanced bioactivity and antibacterial properties," *Journal of Materials Science: Materials in Medicine*, vol. 24, no. 2, pp. 437–445, 2013.

[29] T. G. Peñaflor Galindo, T. Kataoka, S. Fujii, M. Okuda, and M. Tagaya, "Preparation of nanocrystalline zinc-substituted hydroxyapatite films and their biological properties," *Colloid and Interface Science Communications*, vol. 10-11, pp. 15–19, 2016.

[30] I. Karacan, D. Senturk, F. N. Oktar et al., "Structural and characterisation analysis of zinc-substituted hydroxyapatite with wet chemical precipitation method," *International Journal of Nano and Biomaterials*, vol. 6, no. 3-4, pp. 188–204, 2016.

[31] X. S. Nguyen, G. Zhang, and X. Yang, "Mesocrystalline Zn-doped Fe_3O_4 hollow submicrospheres: formation mechanism and enhanced photo-fenton catalytic performance," *ACS Applied Materials & Interfaces*, vol. 9, no. 10, pp. 8900–8909, 2017.

[32] K. M. Lee, C. W. Lai, K. S. Ngai, and J. C. Juan, "Recent developments of zinc oxide based photocatalyst in water treatment technology: a review," *Water Research*, vol. 88, pp. 428–448, 2016.

[33] W. Li, G. Wang, C. Chen, J. Liao, and Z. Li, "Enhanced visible light photocatalytic activity of ZnO nanowires doped with Mn^{2+} and Co^{2+} ions," *Nanomaterials*, vol. 7, no. 1, p. 20, 2017.

[34] F. Ji, C. Li, J. Zhang, and L. Deng, "Efficient decolorization of dye pollutants with $LiFe(WO_4)^2$ as a reusable heterogeneous Fenton-like catalyst," *Desalination*, vol. 269, no. 1–3, pp. 284–290, 2011.

[35] S. Xavier, R. Gandhimathi, P. V. Nidheesh, and S. T. Ramesh, "Comparison of homogeneous and heterogeneous Fenton processes for the removal of reactive dye Magenta MB from aqueous solution," *Desalination and Water Treatment*, vol. 53, no. 1, pp. 109–118, 2015.